Why are *para*-hydrogen clusters superfluid? A quantum theorem of corresponding states study

Mikhail B. Sevryuk,[a] J. Peter Toennies,[b] and David M. Ceperley[c]
Max Planck Institute for Dynamics and Self-Organization, Bunsenstraße 10, 37073 Göttingen, Germany

(Received 23 February 2010; accepted 9 June 2010; published online 10 August 2010)

The quantum theorem of corresponding states is applied to N=13 and N=26 cold quantum fluid clusters to establish where *para*-hydrogen clusters lie in relation to more and less quantum delocalized systems. Path integral Monte Carlo calculations of the energies, densities, radial and pair distributions, and superfluid fractions are reported at T=0.5 K for a Lennard-Jones (LJ) (12,6) potential using six different de Boer parameters including the accepted value for hydrogen. The results indicate that the hydrogen clusters are on the borderline to being a nonsuperfluid solid but that the molecules are sufficiently delocalized to be superfluid. A general phase diagram for the total and kinetic energies of LJ (12,6) clusters encompassing all sizes from N=2 to N=∞ and for the entire range of de Boer parameters is presented. Finally the limiting de Boer parameters for quantum delocalization induced unbinding ("quantum unbinding") are estimated and the new results are found to agree with previous calculations for the bulk and smaller clusters. © *2010 American Institute of Physics*. [doi:10.1063/1.3458640]

I. INTRODUCTION

Small *para*-H_2 clusters are fascinating objects which, despite extensive past theoretical study and a few experiments, provide a number of unresolved riddles. In 1991 path integral Monte Carlo (PIMC) calculations predicted a sizable superfluid fraction in clusters with $N \leq 18$ molecules below about 2 K.[1] As opposed to superfluid ^{4}He clusters, which exhibit flat unstructured radial density profiles consistent with their being liquid, the superfluid pH_2 clusters have structured radial distributions, as expected for solid clusters. This solid-superfluid opposition subsequently stimulated a large number of theoretical studies of the structures of small pH_2 clusters.[2–19] Several authors claim that the small clusters with $N \leq 26$ are liquidlike,[4–9] others call attention to the extensive exchange between different solvation shells.[2,11] On the other hand, diffusion Monte Carlo (DMC) T=0 calculations indicate that N=13 and possibly 19 and 33 are magic and energetically more stable than the neighboring sizes, consistent with the clusters being solidlike.[10,13,17] PIMC calculations at $0.5 \leq T \leq 4.5$ K indicate also that N=19, 23, 26, 29, 32, and 37 clusters are magic in agreement with icosahedral magic numbers expected for solid clusters.[14,16] Other PIMC calculations suggest that below about 0.75–0.25 K the quantum delocalization is greatly enhanced[19,20] favoring superfluidity. The true interpretation of these results is further complicated by finite size effects which smear out the differences between a liquid and a solid and between a normal fluid and a superfluid.

The only *experimental* evidence for superfluidity comes from spectroscopic studies of small *para*-hydrogen clusters attached to a single OCS (carbonyl sulphide) chromophore molecule. These clusters were cooled either to 0.38 K by embedding them in pure ^{4}He droplets or to 0.15 K inside ^{4}He droplets, which in turn were inside a larger ^{3}He droplet. The disappearance of the Q-branch in the infrared spectrum on cooling to 0.15 K for $N \geq 11$ was attributed to the onset of superfluidity.[21,22] This interpretation was confirmed by PIMC calculations of the *free* clusters.[23,24] Neither for *pure* H_2 clusters, nor for the bulk, is there presently any experimental evidence for superfluidity. Although the production and detection of clusters in nozzle beam expansions were first demonstrated with H_2 clusters,[25] presently only limited information is available on their properties. Small pure *para*-H_2 clusters have only been studied in two experiments. Raman spectroscopy confirms the existence of magic 13, 33, and 55,[8,26] while nondestructive matter-wave diffraction experiments, which are also ideally suited for investigating such fragile species, indicate that pure *para*-H_2 clusters are magic at N=13, while the normal H_2 clusters of the same size are not.[27] More extensive experiments are available for larger clusters. Time-of-flight distributions and mass spectra of pure clusters with $N \approx (2 \times 10^3) - (1.4 \times 10^4)$ molecules indicate that these clusters have temperatures of about 3.1 K and are probably liquid.[28,29] Indeed evidence suggests that after heterogeneous nucleation, large clusters solidify internally but appear to have a liquid surface.[29] The liquid nature of large clusters was also confirmed by time resolved VUV fluorescence spectroscopy of embedded Xe atoms.[30] More direct evidence comes from high spatial and spectral resolution Raman spectroscopy which clearly indicates that in the course of the expansion large pH_2 clusters gradually solidified after first being liquid.[8] This was confirmed by a very recent coherent anti-Stokes Raman spectroscopy experiment

[a]Also at Institute of Energy Problems of Chemical Physics, The Russia Academy of Sciences, Leninskiĭ Prospect 38, Bldg. 2, 119334 Moscow, Russia.
[b]Electronic mail: jtoenni@gwdg.de.
[c]Also at Department of Physics, University of Illinois at Urbana-Champaign, Urbana, IL 61801, USA.

which revealed that after expansion, large ($N \approx 10^4$) pure pH_2 clusters are indeed solid, and only approach a liquidlike state if greatly diluted in He gas during the expansion.[31]

The latest proposal to search for superfluidity in pure pH_2 is based on using a jet expanded micron-sized filament of liquid pH_2. The idea is to cool the liquid filament by passing it through a moderator consisting of 1.3 K ^{3}He gas and to detect superfluidity by two-photon Raman excitation.[32]

In the present article, an attempt is undertaken to understand the apparent contradictory behavior of the small pure hydrogen clusters by carrying out a series of path integral Monte Carlo calculations with different values of the potential well depth, values which are both larger and smaller than the accepted value for H_2. In analyzing the data, advantage is taken of the "Quantum Theorem of Corresponding States" (QTCS) originally introduced by de Boer and co-worker[33,34] to account for the dependence of the thermodynamic properties of light systems upon quantum effects. According to QTCS the thermodynamic functions of a class of systems with a pair potential of the form

$$v(r) = \varepsilon v^*\left(\frac{r}{r_0}\right), \tag{1}$$

when expressed in terms of the appropriate reduced dimensionless variables, will be the same for a given value of the de Boer parameter

$$\widetilde{\Lambda^*} = \frac{\lambda(\varepsilon)}{r_0} = \frac{h}{r_0\sqrt{m\varepsilon}}, \tag{2}$$

where $\lambda(\varepsilon)$ is an effective de Broglie wavelength for relative motion of particles with mass m and energy ε. Thus as $\lambda(\varepsilon)$ increases relative to the range of the potential r_0, which is proportional to the average distance between the particles, quantum delocalization becomes increasingly important. Since in recent related studies the quantity $\widetilde{\Lambda^*}/2\pi$ has been used we have adopted this quantity which is denoted here as Λ^*. In addition to the reduced potential v^* and reduced distance, usually denoted by $x=r/r_0$, other important reduced quantities are the densities $\rho^*=\rho r_0^3$ and the various energies such as the total energy $E^*=E/\varepsilon$ and the temperature $T^*=T/\varepsilon$. The dimensionless parameters characterizing a cluster are Λ^*, T^*, and N. However, at a low enough temperature, for many structural properties, we can assume that $T^*=0$.

In these units the Hamiltonian is

$$\frac{H}{\varepsilon} = \frac{\Lambda^{*2}}{2}\sum_{i=1}^{N}\nabla_i^2 + \sum_{1\le i<j}^{N} v^*(x_{ij}). \tag{3}$$

From Eq. (3) we see that Λ^* determines the weight of the kinetic energy relative to the potential energy and has a dramatic effect on the properties. In addition to better understanding superfluidity in *para*-H_2 clusters, the present QTCS study was undertaken to correlate and analyze the effects of quantum delocalization on the microscopic properties such as radial and pair distributions, and the superfluid fraction of the general class of small bosonic quantum clusters.

The simplest realistic potential which satisfies Eq. (1) is the Lennard-Jones (12,6) potential,

$$V(12,6) = 4\varepsilon\left[\left(\frac{r_0}{r}\right)^{12} - \left(\frac{r_0}{r}\right)^{6}\right], \tag{4}$$

where ε is the well depth and r_0 is the distance at which the potential vanishes. The distance of the potential minimum is given by $r_m=2^{1/6}r_0=1.122r_0$. For describing H_2, the Lennard-Jones (LJ) (12,6) potential is less accurate than the frequently used Silvera–Goldman[35] or the Buck *et al.*[36] H_2 potentials or the several recent *ab initio* potentials.[37–39] Its choice was motivated by its simplicity, the ability to model the entire class of rare gas clusters, and the possibility to compare the results with the LJ (12,6) classical calculations of Doye and Wales and collaborators.[40,41] In a parallel study, radial distributions calculated with the LJ (12,6) potential were found to be in very good agreement with those calculated with the Silvera–Goldman and Buck *et al.* potentials.[20]

The variation in Λ^* was implemented by decreasing ε below its accepted value, denoted by ε_0, in three steps (corresponding to an increase in Λ^*) in order to mimic more quantum delocalized, liquidlike clusters. ε was also increased (corresponding to a decrease in Λ^*), to make the clusters more rigid and solidlike. For the simulations two representative cluster sizes were chosen, N=13 and 26. The N=13 cluster has been predicted to be superfluid at $T \le 2$ K despite its possessing an icosahedral structure.[1,16] The N=26 cluster was chosen since it is the smallest cluster for which a sharp drop in the superfluid fraction and the transition temperature to values of about T=0.5 K was found.[14,16]

Several theoretical investigations of the effect of quantum delocalization on the thermodynamic properties of Lennard-Jones clusters have been reported.[41–46] Chakravarty,[42] in the only previous QTCS study of microscopic properties, examined the effect of changing the particle mass on the energies, cluster radius, and density profiles of N=13 and 19 clusters using a LJ (12,6) potential with fixed values of ε and r_0 in the range $0 \le \Lambda^* \le 0.28$. More recently Mandelshtam and collaborators[43–46] explored the melting transitions of Lennard-Jones clusters up to N=147 for $0 \le \Lambda^* \le 0.32$. A detailed study of the influence of quantum delocalization on the melting and premelting of N=19, 31, 38, and 55 Lennard-Jones clusters of the rare gases (except He), D_2, and H_2 was reported by Calvo *et al.*[41]

This article is organized as follows. After a brief description of the computational method, the reduced potential, kinetic, and total energies for N=13 and 26 bosonic clusters are presented as a function of Λ^* spanning from $\Lambda^*=0.202$ up to $\Lambda^*=0.402$. All the present results are for T=0.5 K which is essentially a zero temperature and for low nearly zero pressures unless noted otherwise. The prediction of the reduced properties of ^{4}He clusters ($\Lambda^*=0.398$), which are known to be liquid and superfluid, was confirmed. The new calculations are compared with the only other previous calculations[42] for N=13 and with the predictions for classical clusters ($\Lambda^*=0$).[40,41] An extrapolation to zero total energies yields values for Λ^* at which quantum delocalization is sufficient to unbind the clusters, a process which we call "quantum unbinding." These results are compared with earlier estimates[47,48] and a dependence on $N^{-1/3}$ is found. Next, the radial and pair distributions are presented as a function of

Λ^*. The corresponding calculations for ^{4}He clusters are in excellent agreement. The cluster densities, root mean square distances, and superfluid fractions are described next. By comparing the kinetic and total energies for N=13 and 26 with, at the one extreme, those of dimers (N=2) and with, at the other extreme, the bulk (N=∞) a type of phase diagram covering the entire range of Λ^* for quantum bound clusters is obtained. The article closes with an analysis of the size dependence of the de Boer parameter for quantum unbinding.

The loss of overlap seen in the radial distributions with decreasing Λ^* correlates with a sharp decrease in the superfluid fraction. Thus, it appears that the true potential for H_2 is close to the borderline between a solidlike cluster and one with sufficient overlap between the shells to allow for enough exchange for superfluidity. A small increase in the well depth away from the accepted value would lead to a decrease in quantum delocalization, which would be enough to produce a nonsuperfluid cluster.

II. METHOD

The majority of the present calculations were carried out with a somewhat modified version of the PIMC program originally written by Buch.[49] Since this program does not account for intermolecular exchange it will be referred to as distinguishable PIMC (DPIMC). Although it cannot provide information on the superfluid fraction of the clusters, there is considerable evidence that the effect of exchange on many of the structural properties is very small.[50] Within the present study this was confirmed by a number of comparisons with full PIMC calculations that do include exchange and provide the superfluid fraction. The superfluid fraction is obtained from the formula[51]

$$\mathrm{SF} = \frac{\rho_s}{\rho_{\mathrm{tot}}} = \frac{4m^2\langle A^2\rangle kT}{3\hbar I_{\mathrm{cl}}}, \tag{5}$$

where m is the particle mass, A is the projected area of the paths in the x-y plane entering into the path integral computed as

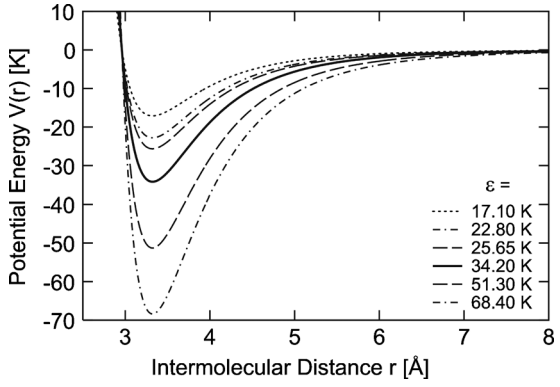

FIG. 1. The Lennard-Jones (12,6) potentials used in the present simulations. All the potentials have identical zero potential range r_0=2.96 Å but differ in the well depth ε from the accepted value of ε_0=34.2 K by factors of 0.50, 0.67, 0.75 and 1.50 and 2.00.

TABLE I. de Boer parameters for H_2 molecules corresponding to the different well depths of a LJ (12,6) potential used in the present simulations. The bold faced values are the accepted values.

ε (K)	68.4	51.3	**34.2** (ε_0)	25.65	22.8	17.1
Λ^*	0.202	0.232	**0.284** (Λ_0^*)	0.328	0.348	0.402

$$A = \frac{1}{2}\sum_{i,j}(\mathbf{r}_{i,j}\times\mathbf{r}_{i,j+1})(\mathbf{r}-\mathbf{r}_{i,j}), \tag{6}$$

and I_{cl} is the classical moment of inertia (MOI),

$$I_{\mathrm{cl}} = \left\langle \sum_{i,j} m_i r_{ij}^{\perp}\cdot r_{i,j+1}^{\perp}\right\rangle. \tag{7}$$

In Eq. (7) $r_{ij}^{\perp}$ and $r_{i,j+1}^{\perp}$ are radial distances from the center of mass perpendicular to the axis of rotation for particle i and j is the index of the imaginary time coordinate.

All the calculations were carried out at sufficiently low temperatures, such that the loss of particles due to evaporation was negligible. For this reason the calculations were only possible for Λ^* well below the extrapolate values for quantum unbinding.

The accepted potential parameters of the reference Lennard-Jones (12,6) potential for H_2 are ε_0=34.2 K and r_0=2.96 Å (r_m=3.32 Å) and the corresponding value of the de Boer parameter, denoted Λ_0^*, is 0.284. These parameters are slightly modified with respect to those reported by Silvera[52] to obtain a better agreement with the potential energies. In the present study ε was increased by factors of 1.50 and 2.00 and reduced by factors of 0.75, 0.67, and 0.50 with respect to ε_0. Figure 1 illustrates the different potentials. Table I lists the corresponding de Boer parameters and Table II lists the potential and de Boer parameters of other particles mentioned in the text.[53] ^{3}He with Λ^*=0.460 has the largest de Boer parameter of all the natural occurring elements and their isotopes. An even larger de Boer parameter of 0.74 is expected in a laser trapped gas of spin-aligned H atoms.[54]

III. RESULTS

A. Energies

Since most of the calculations were carried out with the computationally faster DPIMC program some results listed in Table III were checked for accuracy by comparisons with results from the PIMC program. For Boltzmann particles

TABLE II. Potential and de Boer parameters for atoms and molecules mentioned in the text.

	r_0 (Å)[a]	ε (K)[a]	Λ^*
Xe	3.91	283	0.009
Kr	3.59	202	0.015
Ar	3.37	143	0.026
Ne	2.77	42.3	0.087
D_2	2.96	34.2	0.201
H_2	2.96	34.2	0.284
^{4}He	2.64	10.95	0.398
^{3}He	2.64	10.95	0.460

[a]The potential parameters for Xe, Kr, Ar, and Ne are from Ref. 55.

TABLE III. Comparison of DPIMC and PIMC energies per molecule in Kelvin calculated with two different programs for Boltzmann statistics and for Bose statistics, respectively, using a LJ (12,6) potential with $\varepsilon=34.2$ K ($\Lambda^*=0.284$). The numbers in parentheses are the root standard deviations. The classical moments of inertia I_{cl}, the root mean square areas, and the superfluid fractions (SFs) are also listed.

N	T (K)	Program	Statistics	$-V(N)/N$	$KE(N)/N$	$-E(N)/N$	I_{cl} (amu Å^2)	$(\langle A^2\rangle)^{1/2}$ (Å^2)	SF
13	0.5	DPIMC	Boltzmann	42.97(0.18)	25.59(0.18)	17.38(0.15)	⋯	⋯	0
13	0.5	PIMC	Boltzmann	42.51(0.05)	25.53(0.05)	16.98(0.01)	157.3(0.2)	19.6(0.2)	0
13	0.5	PIMC	Bose	40.79(0.03)	23.45(0.03)	17.30(0.01)	163.5(0.2)	45.3(0.4)	1.03[a]
13	1.5	DPIMC	Boltzmann	43.01(0.28)	25.77(0.27)	17.25(0.25)	⋯	⋯	0
13	1.5	PIMC	Boltzmann	42.52(0.03)	25.83(0.03)	16.69(0.01)	151.9(0.1)	8.43(0.03)	0
13	1.5	PIMC	Bose	40.89(0.03)	23.77(0.03)	17.12(0.02)	155.4(0.2)	23.49	0.89(0.01)
26	0.5	DPIMC	Boltzmann	60.2(0.28)	34.72(0.36)	25.49(0.45)	⋯	⋯	0
26	0.5	PIMC	Boltzmann	59.52(0.01)	34.43(0.01)	25.08(0.01)	465.5(0.2)	21.07(0.3)	0
26	0.5	PIMC	Bose	55.08(0.04)	29.88(0.04)	25.22(0.01)	485(1.0)	76.7(1.0)	0.95

[a]Because of numerical errors the SFs are occasionally greater than one.

both programs agree within the accuracy of the statistical errors of about 2%. The potential and kinetic energies for Bose particles are, however, significantly smaller (≈4%–12%) in absolute values than for Boltzmann particles, but since they contribute to the total energies with opposite signs, the total energies are nearly identical.

The DPIMC total energies for the reference Lennard-Jones potential at 1.5 K were compared with DMC (T=0 K) calculations[10] for the potential of Buck *et al.* For all sizes the DPIMC Lennard-Jones energies are significantly smaller by as much as 37% for N=4 decreasing to about 19% for N=40. Since the total energies calculated for Boltzmann and Bose particles are nearly identical, the inclusion of exchange cannot explain the discrepancies. The differences are also much larger than can be explained by temperature. The increase in energy calculated from the elementary excitation energy levels[56] is only about 0.06 K for N=13 and 0.5 K for N=26. Since similar differences in total energy were also reported by Chakravarty[57] for $(pH_2)_{13}$ at 2.5 K the differences in energy are attributed to the different potentials used.

Tables IV–VII in the Appendix contain the main results for the calculated reduced energies, moments of inertia, and superfluid fractions for the N=13 and N=26 clusters each at two temperatures of 0.5 and 1.5 K for five or six values of $\varepsilon/\varepsilon_0$ and Λ^*. Results are presented for Boltzmann particles calculated with the DPIMC program as well as for Bose particles calculated with the PIMC program. The compari-

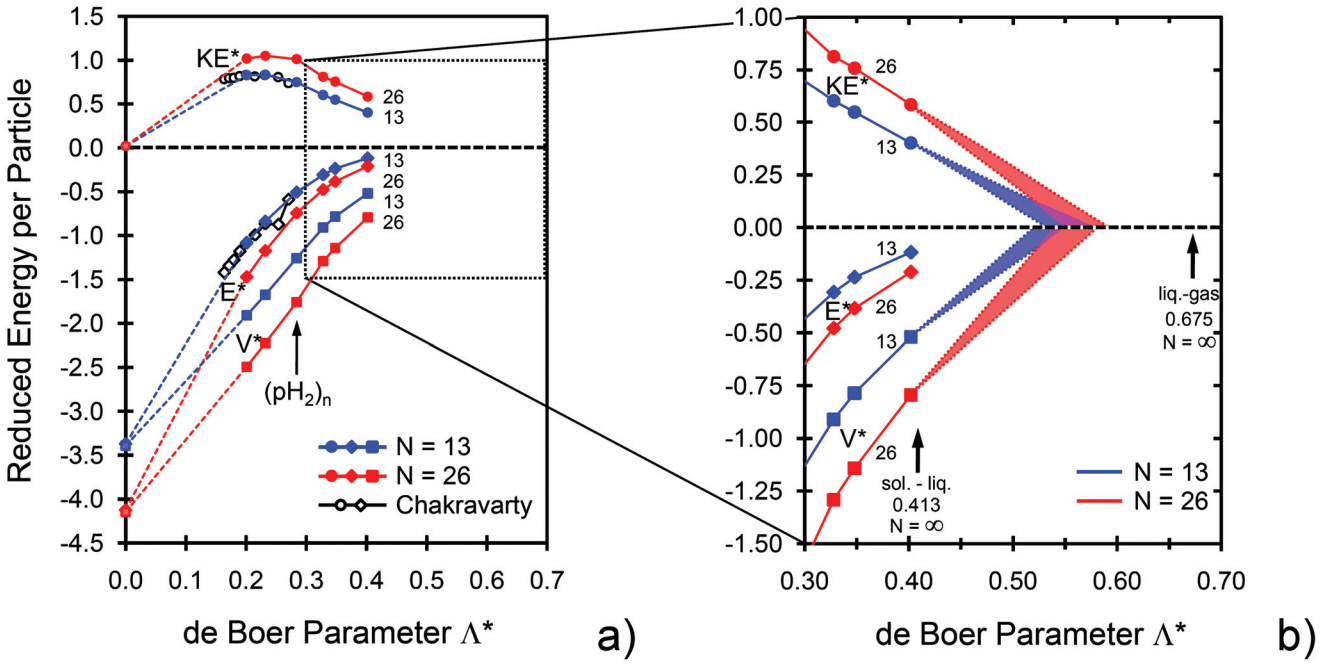

FIG. 2. (a) The reduced kinetic, potential, and total energies per molecule at T=0.5 K are plotted vs the de Boer parameter Λ^*. The potential energies extrapolate to the values for classical clusters at $\Lambda^*=0$. The results of Chakravarty for KE^* and V^* per molecule for an N=13 cluster are shown as open symbols (Ref. 42). The enlarged section (b) illustrates the extrapolation to vanishing kinetic and potential energies. The bulk liquid-gas transition at $\Lambda^*=0.675$ was reported by Miller *et al.* (Ref. 59).

sons reveal an interesting trend with Λ^*. For $\Lambda^* \geq \Lambda_0^*$ the Bose clusters are more stable than the Boltzmann clusters, but for $\Lambda^* < \Lambda_0^*$ corresponding to $\varepsilon > \varepsilon_0$ the opposite is the case. The same trend is found for N=13 and 26 at both temperatures. This suggests that the inclusion of exchange stabilizes the less tightly bound more liquidlike clusters, but destabilizes the tightly bound more solidlike clusters. This seems reasonable since the increased delocalization provided by exchange is expected to have a greater effect for the more liquidlike clusters.

Figure 2(a) displays the present DPIMC results for the reduced energies per particle as a function of the de Boer parameter at 0.5 K. As discussed above, the effect of temperature is hardly noticeable on the scale of the figure. The present results are in reasonable agreement with the reduced kinetic and total energies of Chakravarty[42] for N=13 in the range $0.1 \leq \Lambda^* \leq 0.28$ and $T^*=0.1$, which are shown as open symbols in Fig. 2(a).

Especially noteworthy is the nearly linear increase of the reduced potential energies with Λ^* for both N=13 and N=26. It is well known that thermodynamic bulk properties, such as the heat of evaporation, scale linearly with ε. The calculated potential energies when extrapolated linearly to $\Lambda^*=0$ give energies which agree almost perfectly with the classical reduced energies of the corresponding Lennard-Jones clusters.[40,41] For Λ^* less than about 0.3 the dependence of the reduced potential energy is given by

$$\frac{V^*(\mathrm{N})}{\mathrm{N}} = \frac{V_{\mathrm{cl}}^*(\mathrm{N})}{\mathrm{N}} + A_V(\mathrm{N})\Lambda^*, \quad \Lambda^* \leq 0.3, \tag{8}$$

where the second term accounts for the quantum correction. A best fit of the calculated points yields $A_V(13)=7.75$ and $A_V(26)=8.88$. The slight decrease in the slope beyond $\Lambda^*=0.3$ seen for both sizes suggests that terms higher than the linear term in Λ^* begin to make a noticeable contribution. Because of these higher order terms it is not straightforward to extrapolate $V^*(\mathrm{N})/\mathrm{N}$ to 0. At the corresponding value of Λ^* the cluster will be fully disintegrated since the effective binding potential has vanished. We call this process, which was first explored for N=2–5 by Nightingale and colleagues,[48] *quantum unbinding*. Figure 2(b) shows an approximate extrapolation based on the combination of several analytic functions as well as by eye. $V^*(\mathrm{N})/\mathrm{N}$ vanishes at about $0.52 \leq \Lambda_{\mathrm{qu}}^* \leq 0.56$ for N=13 and for N=26 at slightly larger values of $0.54 \leq \Lambda_{\mathrm{qu}}^* \leq 0.58$, where the index qu denotes quantum unbinding. In general the Λ^* for stability of a cluster of size N requires that at this Λ^*, one has $E^*(\mathrm{N}) \leq E^*(M)$ for all $M < \mathrm{N}$. Quantum unbinding occurs when, for example, $E^*(\mathrm{N}-1)=E^*(\mathrm{N})$, or in other words for the value of Λ^* at which the chemical potential vanishes.

The reduced kinetic energies show a more complicated behavior consisting of a rise to a maximum, followed by a gradual decline. For N=13 the present values match well with the earlier work by Chakravarty[42] in the range of $0 \leq \Lambda^* \leq 0.28$ for a reduced temperature of $T^*=0.1$ (T=3.42 K). The present kinetic energies have a maximum at about $\Lambda^* \approx 0.23$, which was also noted by Chakravarty, and then fall off nearly linearly with further increasing Λ^*. The new data and the earlier results for N=13 and the classical Monte Carlo calculated value[58] for T=0.5 K of $KE_{\mathrm{cl}}^*(13)/13=0.020$ fit approximately a cubic polynomial,

$$\frac{KE^*(13)}{13} = \frac{KE_{\mathrm{cl}}^*(13)}{13} + A_{KE}(13)\Lambda^* + B_{KE}(13)\Lambda^{*2} + C_{KE}(13)\Lambda^{*3}, \tag{9}$$

with the result $A_{KE}(13)=7.4$, $B_{KE}(13)=-22.8$, and $C_{KE}(13)=14.9$. Different extrapolations to $KE^*(13)/13=0$ yield values for quantum unbinding of $0.53 \leq \Lambda_{\mathrm{qu}}^* \leq 0.57$. A similar fit of the data for N=26 using the classical Monte Carlo value at T=0.5 K of $KE_{\mathrm{cl}}^*(26)/26=0.059$ was less satisfactory. For N=26 different extrapolations lead to somewhat larger values of $0.55 \leq \Lambda_{\mathrm{qu}}^* \leq 0.59$. Because of the greater curvature of the total energy curves no attempt was made in this case to extrapolate to zero, but since the total energy is the sum of the kinetic and potential energies the extrapolated values will be very similar.

Chakravarty[42] attributed the maximum in the kinetic energy at about $\Lambda^* \approx 0.23$ to the increasing influence of metastable local minima with high potential which are accessed as Λ^* is increased. If her explanation is correct, the potential energy, which was not reported by Chakravarty, should exhibit a marked deviation from the linear behavior at about the same values of Λ^*, which was not found here. Instead we attribute the maximum to competing effects. At small Λ^* the increase in zero point energy is the dominant effect. Then with further increase in Λ^*, the decrease in particle density to be discussed in Sec. III B is the over-riding effect. This decrease in particle density tends to lower the zero point energy since the average potential energy between the more dispersed molecules also decreases. Beyond $\Lambda^* \approx 0.23$, this decrease ultimately leads to the vanishing of the kinetic energy.

The 0.5 K energies interpolated to $\Lambda^*=0.398$ were checked by comparing with calculations for ^{4}He clusters of the same size. In order to avoid too much evaporation temperatures of T=0.5 K ($T^*=0.046$) and 0.25 K ($T^*=0.023$) were chosen. At 0.5 K the evaporative loss of ^{4}He atoms is small and at 0.25 K entirely negligible. The calculated potential energies for N=13 ^{4}He clusters at 0.5 K (0.25 K) are −0.534 K (−0.557 K) and for N=26 −0.829 K (−0.836 K), exhibiting only a small temperature dependence. These values compare well with linearly interpolated values of −0.538 and −0.816 K ($T^*=0.029$) within the errors of the two calculations. Evaporation has a larger effect on the total energies. For N=13 the total energy for a ^{4}He cluster at T=0.5 K (0.25 K) is −0.0906 K (−0.122 K) and for N=26 it is −0.184 K (−0.212 K) compared to interpolated values of −0.126 and −0.223 K, respectively.

We are aware of only one previous study of quantum unbinding of small Lennard-Jones clusters by Nightingale and collaborators.[48] They investigated the dependence of the total energy and average geometric size on $m^{-1/2}$, which is proportional to the de Boer parameter and established effective masses for what they call the *unbinding transition* for clusters with N=2, 3, 4, and 5. They also observed a shift in the de Boer parameter to larger values with increasing N. Also, in essential agreement with our results, they predict that the cluster energy is linear in the de Boer parameter in

both the classical and extreme quantum limits.

Nosanow and co-workers[59,60] investigated the behavior of the reduced total energy of a bulk LJ Bose fluid at zero pressure and temperature and reported a zero energy intercept at $\Lambda^*=0.675$, which marks what they called the *liquid-gas transition*. Their value, which is shown in Fig. 2(b), is larger than the values found here for the small clusters. This is expected since the total energy per particle invariably increases with cluster size. These bulk and related predictions of quantum unbinding for small clusters by Nightingale and collaborators[48] are compared with the present results in Sec. III F.

It is interesting to note that a process somewhat related to quantum unbinding was observed in solid helium by de Boer and Blaisse[34] in their QTCS analysis: "The deviations from the classical value (of the volume) may be fully explained by the effect of the zero point energy which exerts a repulsive pressure in the solid state, 'blowing it up,' thus giving a relative larger volume, the larger the values of Λ^* are and giving a corresponding lower energy as the molecules are forced out of the low energy positions."

Miller *et al.*[59] also reported that the bulk LJ Bose solid undergoes a solid-liquid transition at $\Lambda^*=0.413$, which is also indicated in Fig. 2(b). Since small clusters are less tightly bound the melting transition is expected to be shifted to smaller values of Λ^* depending on their size. Chakravarty observed the smeared out melting transition at $T^*=0.1$ to begin at $\Lambda^*=0.189$ for N=13 and for N=19 at $\Lambda^*=0.215$ extending to larger Λ^* by about $\Delta\Lambda^*=0.8$.[42] A linear extrapolation (using ε_0 for H_2) to $T^*=0.0146$ (T=0.5 K) yields for N=13 a range extending from $\Lambda^*=0.26$ up to about 0.34 for the melting transitions. Accordingly the H_2 clusters ($\Lambda^*=0.284$) lie within the predicted melting region.

B. Radial density distributions

The changes in the radial density (i.e. the angle averaged density about the center of mass) and two-body pair distributions provide complementary microscopic information on the influence of quantum effects. Figure 3 illustrates the effect of quantum delocalization upon the DPIMC radial distributions of the N=13 cluster at T=0.5 K. In the classical limit, the cluster consists of a central molecule and an icosahedral shell of 12 molecules equally distributed over a shell with radius of $R=3.20$ Å,[40] which is indicated by a vertical line in Fig. 3(a). At the smallest value of $\Lambda^*=0.202$ the shell distribution is only somewhat broadened and slightly shifted outwards with respect to the classical radius but there is no overlap with the central molecule [Fig. 3(a)]. A small overlap is first seen for $\Lambda^*=\Lambda_0^*$, at which point some exchange between the central molecule and outer shell probably occurs in the real clusters. Figure 3(b) shows the dramatic broadening of both the central and outer peaks for $\Lambda^*>\Lambda_0^*$. At $\Lambda^*=0.328$ the minimum is nearly completely washed out and at the largest $\Lambda^*=0.402$ the density is flat over the entire range starting at the origin and falls off to its half density at about $R_{0.5}=5.7$ Å or in reduced units at $R_{0.5}^*=1.93$. Thus an N=13 H_2 cluster with $\Lambda^*=0.402$ is completely quantum melted to form a quantum liquid. A comparison of the reduced radial density distribution calculated for $\Lambda^*=0.402$ is in excellent agreement with the reduced radial density distribution calculated for a LJ ^{4}He cluster ($\Lambda^*=0.398$).

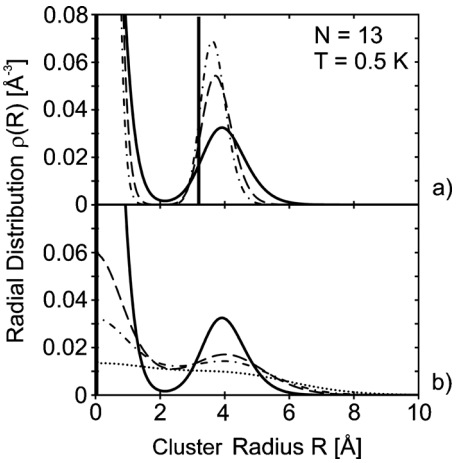

FIG. 3. (a) The radial density distributions for an N=13 cluster at T=0.5 K: $\Lambda^*=0.202$ (---), $\Lambda^*=0.232$ (-·---), and $\Lambda^*=\Lambda_0^*$ (—). (b) The radial density distributions for $\Lambda^*=\Lambda_0^*$ (—), $\Lambda^*=0.328$ (---), $\Lambda^*=0.348$ (-·---), and $\Lambda^*=0.402$ (····). The vertical line at 3.20 Å indicates the position of the 12 particles making up the outer shell of a classical icosahedral cluster with $\varepsilon=\varepsilon_0$. The distributions are normalized to give unity: $\int_0^{10\ \text{Å}}\rho(R)R^2dR=1$. Multiplication of $\rho(R)$ by $4\pi/N$ gives the density in number of molecules per Å^3.

Figures 4(a) and 4(b) display the corresponding results for an N=26 cluster at T=0.5 K. The same trends are seen for the larger cluster as for the N=13 cluster. The classical structure consists of four shells and is much more complicated than for the pure N=13 icosahedron. It can be looked upon as an icosahedron plus a six-molecule cap upon which four- and three-particle caps are attached. Already at the smallest Λ^*, quantum delocalization is sufficient to smear out the gaps between the shells to such an extent that only three maxima remain [Fig. 4(a)] so that judging by their overlap, extensive exchanges between all the shells are possible. As with the N=13 cluster the shells are shifted outward by

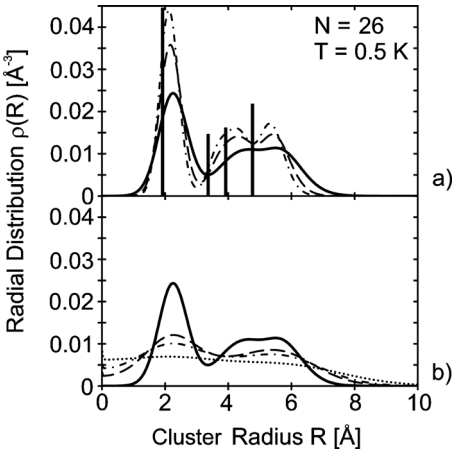

FIG. 4. (a) The radial density distributions for an N=26 cluster at T=0.5 K: $\Lambda^*=0.202$ (---), $\Lambda^*=0.232$ (-·---), and $\Lambda^*=\Lambda_0^*$ (—). (b) The radial density distributions for $\Lambda^*=\Lambda_0^*$ (—), $\Lambda^*=0.328$ (---), $\Lambda^*=0.348$ (-·---), and $\Lambda^*=0.402$ (····). The vertical lines indicate the positions of the shells of a classical cluster with $\varepsilon=\varepsilon_0$.

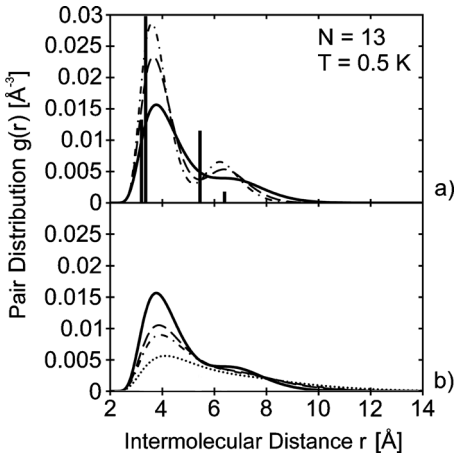

FIG. 5. The pair distribution functions for an N=13 cluster at T=0.5 K. The curves are for the same Λ^* as in Figs. 3 and 4: (a) for $\Lambda^* \leq \Lambda_0^*$ and (b) for $\Lambda^* \geq \Lambda_0^*$. The vertical lines show the classical pair distances. The distributions are normalized to give unity: $\int_0^{15\ \text{Å}} g(r) r^2 dr = 1$.

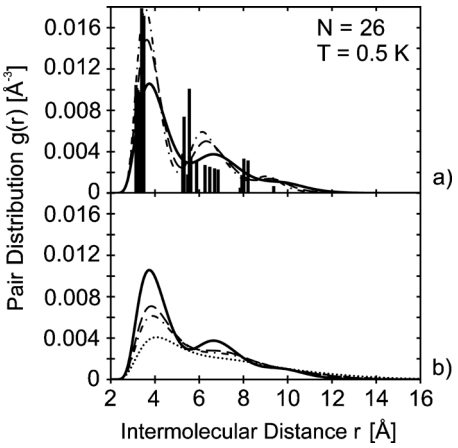

FIG. 6. The pair distribution functions (normalized as in Fig. 5) for an N=26 cluster at T=0.5 K. The curves are for the same Λ^* as in Figs. 3 and 4: (a) for $\Lambda^* \leq \Lambda_0^*$ and (b) for $\Lambda^* \geq \Lambda_0^*$. The vertical lines show the classical pair distances.

about 5% increasing with Λ^* to about 10%, while at the same time, the two outer shells gradually merge together.

In this connection it is noted that the present authors, together with Warnecke *et al.*,[20] recently called attention to the existence of three shells in large hydrogen clusters ($18 \leq N \leq 31$) at 1.5 K where previous DMC (T=0 K) calculations had identified only two shells.[10] This difference was attributed to the different temperatures, a phenomenon which has been designated *quantum melting* but may, in fact, be related to the onset of superfluidity at the lower temperature.[6,14,20] In analogy, the gradual disappearance of structures with decreasing ε and increasing Λ^* found here might be called *potential melting*.

When Λ^* is greater than Λ_0^* the two peaks are completely smeared out and the density distribution again approaches the flat shape of a liquid ^{4}He cluster. The distribution shown for $\Lambda^*=0.402$ is in nearly perfect agreement with that calculated for a ^{4}He cluster.

C. Pair distributions

Another distribution of interest is the two-body or pair distribution function. These DPIMC calculated distributions are plotted in Fig. 5 (N=13) and Fig. 6 (N=26) at T=0.5 K. For both sizes, even for the smallest values of Λ^*, the classical distributions are almost completely smeared out so that the many peaks in the classical distributions are reduced to two peaks. With increasing Λ^* the central major peak gradually shifts to larger distances much in the same way as found for the radial distributions. For $\Lambda^* > \Lambda_0^*$ the two peaks collapse to one central peak. For the largest Λ^* the distributions approach the shape predicted for the same sized ^{4}He clusters.

D. Cluster densities

From the radial density distributions it is possible to obtain information on the cluster particle densities. Since the reduction of the average density in small clusters, which is due to the dominance of the surface region, explains the superfluidity of small clusters, the density is of special interest in order to understand the superfluidity of pH_2 clusters.

The average particle density of a cluster can be expressed as

$$\rho(N) = \frac{N}{\frac{4}{3}\pi R_e^3}, \tag{10}$$

where R_e is the effective sharp radius of an equivalent cluster with a constant density ρ_0. R_e is related to the cluster mean square radius R_c (measured from the cluster center of mass) by

$$R_e^2 = \tfrac{5}{3}\langle R_c^2 \rangle, \tag{11}$$

where $\langle R_c^2 \rangle$ is calculated from the radial distribution $\rho(R)$,[61]

$$\langle R_c^2 \rangle = \frac{4\pi \int_0^\infty R^2 \rho(R) R^2 dR}{4\pi \int_0^\infty \rho(R) R^2 dR}. \tag{12}$$

$\langle R_c^2 \rangle$ is also of interest since it is directly proportional to the cluster MOI [see Eq. (7)].

The reduced particle densities calculated from Eqs. (10)–(12) are plotted in Fig. 7. The classical densities plotted on the left hand ordinate scale for $\Lambda^*=0$ in Fig. 7 were also calculated in the same manner using radial distributions for

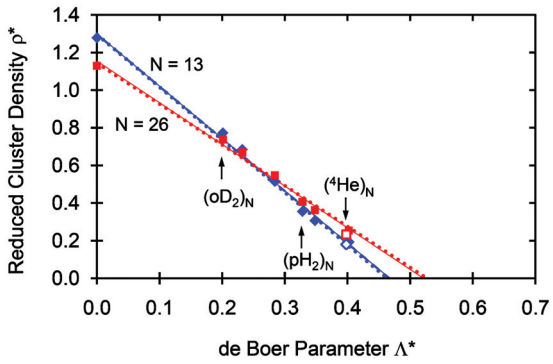

FIG. 7. The reduced particle density $\rho^* = \rho r_0^3$ is plotted as a function of the de Boer parameter for N=13 and N=26 clusters. The classical values shown for $\Lambda^*=0$ are calculated for T=0.5 K. The reduced densities at $\Lambda^*=0.398$ (open symbols) are calculated for ^{4}He clusters.

T=0.5 K calculated with the same DPIMC program starting from the classically calculated coordinates of the cluster particles reported by Wales and collaborators.[40] The classical reduced density at T=0.5 K for N=13 is $\rho^*_{cl}(13)=1.28$, which is only slightly smaller than the value at T=0 K. At T=0.5 K, $\rho^*_{cl}(26)=1.13$.

Figure 7 shows that quantum delocalization leads to a nearly linear decrease in the cluster density with increasing de Boer parameter. In the case of H_2 clusters (with ε_0) the reduced density is about one-third the density of the corresponding classical clusters, but about twice that of the ^{4}He clusters. This indicates that the radial distributions are more spread out compared to the classical distributions by a factor $2^{1/3}$ as found in a recent related DPIMC, DMC study.[20] Both curves in Fig. 7 could be reasonably well fitted with a linear dependence on Λ^*,

$$\rho^*(13,26) = \rho^*_{cl}(13,26) + A_\rho(13,26)\Lambda^*, \tag{13}$$

with parameters $\rho^*_{cl}(13)=1.30$, $A_\rho(13)=-2.78$, $\rho^*_{cl}(26)=1.15$, and $A_\rho(26)=-2.22$. In contrast to the energies, the densities for N=13 and 26 lie close together and differ only slightly in their slopes. This suggests that the densities for other sizes may not be very different.

The extrapolation of the best fit curves to $\rho^*=0$ yields the following values for quantum unbinding: $\Lambda^*_{qu}(13)\cong 0.47$ and $\Lambda^*_{qu}(26)\cong 0.52$. These values are significantly smaller than those obtained in Sec. III A from an extrapolation of the potential and kinetic energies (Fig. 2). Since the potential and kinetic energies converged nicely to about the same values it appears that the extrapolations of Fig. 7 are less reliable and the assumed functional form is inadequate as Λ^* approaches Λ^*_{qu}. This would be explained if beyond about $\Lambda^*=0.402$ the radial distributions are less spread out than expected from a simple extrapolation and, consequently, the densities also fall off less rapidly with increasing Λ^*.

Of some interest in this connection is the work of Apenko[62] who estimated the superfluid transition temperature as a function of density for bulk hydrogen assuming that one could prevent it from freezing at low temperatures. According to his estimates, the superfluid transition temperature initially increases with density as for an ideal boson gas but then passes through a maximum at a reduced particle density of $\rho^*=\rho r_0^3=0.3$ and then gradually decreases. For the small H_2 clusters studied here, which are predicted to be superfluid, the reduced densities of about $\rho^*=0.4$ (Fig. 7) are only about 30% greater than the Apenko value and considerably smaller than in the bulk liquid at the triple point ($\rho^*=0.67$).[63] As seen in Fig. 7 compared to the same sized ^{4}He clusters the H_2 reduced densities are about a factor 2 greater.

From the calculated pair distributions $g(r)$ the average root mean square distances between molecules $\langle r_p^2\rangle^{1/2}$ were calculated using an expression analogous to Eq. (12). Also the classical values were calculated using the data in Ref. 40 following the same prescription. The results for both $\langle r_p^2\rangle^{1/2}$ and $\langle R_c^2\rangle^{1/2}$ are plotted in Fig. 8 as a function of Λ^*. The ratio $\langle r_p^2\rangle^{1/2}/\langle R_c^2\rangle^{1/2}$ is equal to $\sqrt{2N/(N-1)}$ and is 1.47 for N=13 and 1.44 for N=26.[64] Initially for small Λ^*, the distances increase linearly but beyond about $\Lambda^*\approx 0.20$, start increasing more rapidly. Beyond the largest value of Λ^* =0.402, both curves are expected to increase sharply since in the limit of quantum unbinding, they should approach infinity. Nightingale *et al.*[48] also observed a sharp increase in size as Λ^* approaches Λ^*_{qu}.

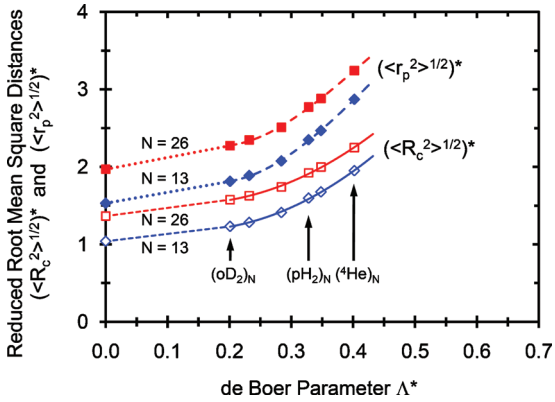

FIG. 8. The reduced root mean square average distances between molecules $(\langle r_p^2\rangle^{1/2})^*$ and the reduced root mean square average distances from the center of mass $(\langle R_c^2\rangle^{1/2})^*$ are plotted as a function of the de Boer parameter for N=13 and N=26 clusters.

It is interesting to note that the average root mean square distances $\langle r_p^2\rangle^{1/2}$ are larger by more than a factor of 2 than the lattice constant a in solid hcp H_2 of 3.78 Å ($a^*=1.27$). Also, the average distances increase significantly in the region of $\Lambda^*\geq 0.26$, where as mentioned earlier, the N=13 cluster begins to undergo quantum induced melting.[42]

E. Superfluid fraction

The dependence of the superfluid fraction upon Λ^* is shown in Fig. 9(a) for an N=13 cluster at T=0.5 and 1.5 K. In previous work, the N=13 cluster was found to have a significant superfluid fraction at temperatures as high as 2 K

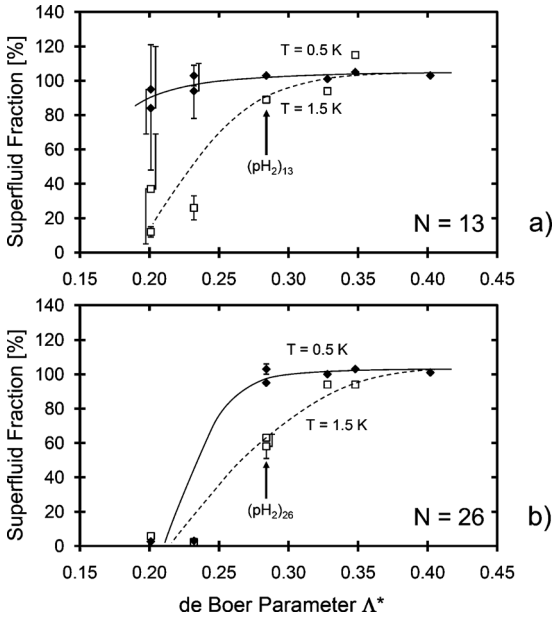

FIG. 9. The superfluid fraction is plotted vs the de Boer parameter Λ^*. (a) compares the superfluid fraction at T=0.5 K and 1.5 K for an N=13 cluster. (b) shows a similar comparison for an N=26 cluster. As expected He clusters ($\Lambda^*=0.398$) are 100% superfluid. Values of the superfluid fraction greater than one are due to numerical errors.

(Refs. 1 and 16) even though it is an especially stable magic number cluster. This is confirmed by the present results, which show that despite the complete suppression of exchanges between the central molecule and the 12 particle outer shell, as seen in the radial distributions, this cluster remains superfluid at T=0.5 K even down to the smallest value of $\Lambda^*=0.202$. The extensive overlap of the pair distributions (Fig. 5), on the other hand, suggests that the intraring exchanges among the molecules in the outer shell at this temperature are sufficient for superfluidity as reported in Ref. 16. In contrast, at the higher temperature of 1.5 K the superfluid fraction drops off sharply as Λ^* decreases below the true value for pH_2. At this temperature, the de Boer parameter is just at the borderline for the N=13 cluster to become "normal" (i.e., nonsuperfluid). It is interesting to see that the greater superfluid fraction in the region of small Λ^* at 0.5 K compared to 1.5 K is consistent with the recently reported reduction in the number of shells in the radial distribution on lowering the temperature.[20]

The N=26 cluster [Fig. 9(b)] shows a similar but less extreme behavior. Previously the present authors, together with Khairallah,[16] reported a superfluid fraction of about 50% at 0.5 K. The larger values found here are attributed to the use of a Lennard-Jones potential instead of the more realistic Silvera–Goldman potential used in Ref. 16. In the earlier study, the superfluid fraction disappeared at 1.0 K. This was attributed to the magic stability of N=26 since a similar strong dependence on temperature was not found for the adjacent N=25 and 27 clusters. The present results at 0.5 K indicate that the N=26 cluster is very close to being normal. In this case, however, the sharp decrease is not explained by an obvious reduction in overlap between the shells in the radial distributions [Fig. 4(a)] nor in the pair distributions [Fig. 6(a)].

F. Cluster size dependence of the energies and quantum unbinding

The present calculations provide a comprehensive overview of the thermodynamic microscopic properties of bosonic clusters at essentially zero pressure and temperatures. The results for N=13 and N=26 can be placed in a broader perspective by considering the known properties of the five rare gases Xe, Kr, Ar, Ne, and He, D_2, and H_2 in the bulk (N=∞) and as dimers (N=2). Figure 10 presents an overview of the reduced total energies (bottom part) and the reduced kinetic energies per particle (upper part) for the entire range of Λ^* from the classical limit $\Lambda^*=0$ to the bulk quantum unbinding limit $\Lambda^*=0.675$.

The bulk total energies at the bottom part of Fig. 10 were taken from recent data for He,[65] H_2,[66] D_2,[66] Ne,[67] Ar,[68] Kr,[68] and Xe[68]. These energies were reduced using the modern values for ε in Table II.[69] Beyond $\Lambda^*=0.413$ the bosonic LJ bulk solid is predicted to be liquid.[60] The curve for the liquid between $\Lambda^*=0.413$ and $\Lambda^*=0.675$ at which the gas-liquid transition occurs is taken directly from Ref. 59.

The dimer data for Xe_2,[70] Kr_2,[70] and Ar_2,[70] Ne_2,[71] and for $(D_2)_2$ and $(H_2)_2$[38] were taken from recent state-of-the-art *ab initio* calculated van der Waals potential curves and the

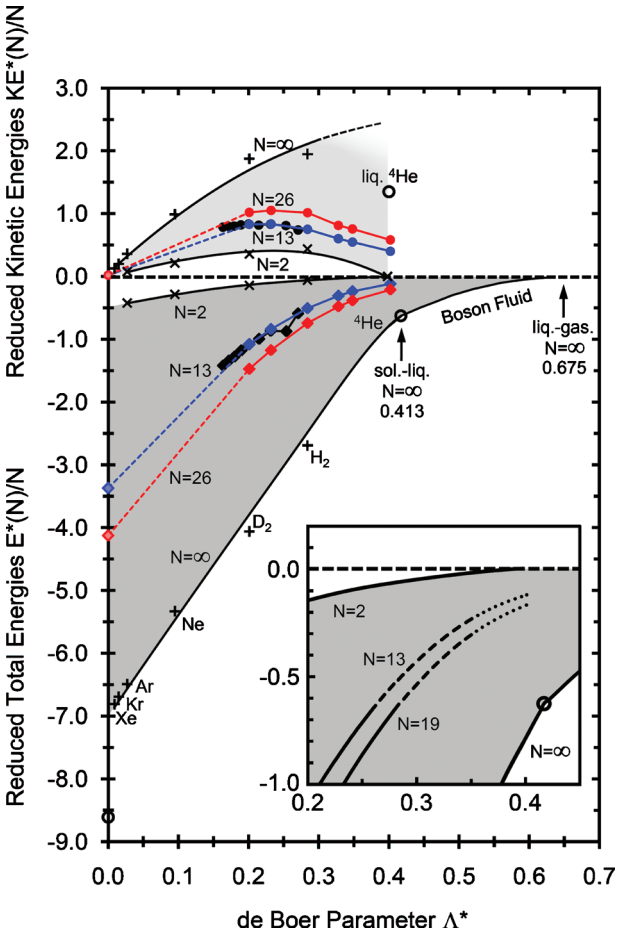

FIG. 10. The zero temperature reduced total energies per particle of bosonic bulk and dimers are plotted as a function of the de Boer parameter and compared with the present T=0.5 K calculations for N=13 and 26. The long-dashes curve sections for N=13 and N=19 in the inset show the range in Λ^* between the beginning and end of the Lindemann index changes of the solid-liquid transition (Ref. 41). Top part: reduced zero temperature kinetic energies per particle for the same substances. The dotted line and fading of the colored region beyond $\Lambda^*\approx 0.3$ reflect the fact that helium is a liquid at P=0 and T=0.

calculated $v=0$ ground state energies which yield D_0^0, the dissociation energy at zero pressure and temperature. In the classical limit there is no zero point energy and since then $D_0^0=\varepsilon$ the reduced total energy is given by $E^*(2)/2=1/2$. For the dimers the correct value for Λ_{qu}^* is very well approximated by setting it equal to Λ^* for He since the helium dimer is known to have a binding energy of less than about 1.3×10^{-3} K.[72,73] An increase in the well depth by about this miniscule amount would be sufficient to break up the dimer. The corresponding effect on the de Boer parameter for He ($\Lambda^*=0.398$) is entirely negligible.

The inset in Fig. 10 shows the information available on the quantum melting of small LJ clusters in relation to the bulk. As mentioned earlier the only values available are from Ref. 42 for N=13 and N=19. We have extrapolated Chakravarty's data at $T^*=0.1$, 0.15, and 0.2 to $T^*=0.014$. For N=13 the extrapolated Lindemann index starts to rise at $\Lambda_m^*=0.26$ and levels off again at $\Lambda^*=0.34$. For N=19 the rise starts at 0.28 and ends at about 0.36. It is interesting to observe that the reduced total energies all lie above about −0.6.

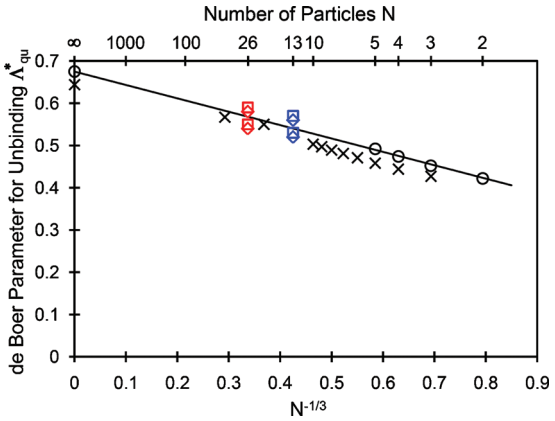

FIG. 11. The de Boer parameter for quantum unbinding is plotted as a function of $N^{-1/3}$. The data for N=13 and 26 [(□) and (◇)] are from the extrapolations in Sec. III A. The data (○) for N=2, 3, 4, and 5 were reported in Ref. 48. The point (0) at $N^{-1/3}=0$ is for the bulk (Ref. 59). The other data (×) are for a realistic tritium dimer triplet potential (Ref. 47). Their value for Λ^*_{qu} at $N^{-1/3}=0$ is a lower bound.

This suggests that possibly the melting of quantum fluid clusters of all sizes sets in as their reduced total energies exceed about −0.6.

The upper part of Fig. 10 shows the kinetic energies. The dimer values plotted are the zero point vibrational energies taken from the same references listed above. The N=∞ points are based on the formula $KE=\frac{9}{16}\Theta_D$, where Θ_D is the Debye temperatures. The total zero point energy of a solid is generally given by $\frac{9}{8}\Theta_D$,[34] but of this amount, only one-half is kinetic and the other half potential energy according to the virial theorem assuming harmonic vibrations. Since helium only becomes a solid above about 25 bars the kinetic energy of the liquid[74] is shown in Fig. 10. The Debye temperatures for Xe, Kr, Ar, Ne, and He are from Ref. 75 and the data for H_2 and D_2 from Ref. 76.

We are aware of only two previous studies of quantum unbinding of small clusters. For a LJ (12,6) Nightingale and collaborators[48] reported values of a critical mass m_c for unbinding for N=2, 3, 4, and 5. Since they used reduced units in which $\hbar=1$, $\varepsilon=1$, and $r_0=2^{-1/6}$ in their notation $\Lambda^*_{qu}=2^{1/6}\ m_c^{-1/2}$. Hanna and Blume[47] also reported critical masses but for the triplet tritium dimer potential for 3…(1)…10, 20, and 40. Figure 11 compares the present results for N=13 and 26 with these previous determinations and the values of $\Lambda^*_{qu}=0.675$ for the bulk (N=∞) (Ref. 59) as a function of $N^{-1/3}$. It is gratifying to see that all the results lie on a straight line which extrapolates to the bulk value.[59] The decrease in Λ^*_{qu} with decreasing size reflects the reduced overall binding of the clusters as the coordination is reduced. As opposed to more classical clusters, where the surface atoms evaporate first before the inner core falls apart, in the case of quantum unbinding, the entire cluster disintegrates all at once since a cluster with N−1 particles is less bound than an N-particle cluster.

IV. SUMMARY

The present article describes a systematic application of the QTCS to the investigation of the effect of quantum delocalization on the energies and microscopic properties, such as radial and pair distributions, of finite-sized ultracold bosonic clusters. This study represents a major extension of the only previous similar investigation by Chakravarty.[42] Although the results reported here are quite general, the main goal was to understand the apparent contradiction between the superfluidity of small *para*-H_2 clusters and their structured radial distributions as well as their predicted and partly observed magic numbers. Whereas superfluidity suggests that the clusters are liquid, the latter properties are consistent with the clusters being solid. The calculated radial and pair distributions reported reveal that the LJ (12,6) clusters with the accepted potential parameters for H_2 lie very close to being solids, but still exhibit sufficient overlap to provide for their superfluidity, as confirmed by the calculated superfluid fractions. With the increase of the well depth with respect to the accepted value, the superfluid fraction drops off sharply. This delicate competition between solid and liquid behaviors also explains the sharp drop-off in the superfluid transition temperature found previously for clusters larger than N=25.[6,14,16] Beyond N=25 the strength of the average potential increases as the effect of the reduced coordination at the surface diminishes and quantum delocalization is no longer sufficient for superfluidity.

Although QTCS was originally formulated to describe thermodynamic bulk properties, the present results demonstrate that it can also be useful for understanding microscopic properties such as the radial and pair distributions of quantum clusters. As presently formulated, QTCS does not explicitly account for the dependence of the energies on size and more work is needed to identify such dependence. Finally we mention that the present QTCS calculations may be of interest in connection with recent experiments to create marginally bound bosonic aggregates via Feshbach resonances in magnetic fields.[77] As first pointed out by Palmer and Anderson[78] QTCS is also of interest for understanding nuclear and neutron-star matter. Although nuclear potentials, such as the Yukawa potential, are softer and broader than LJ (12,6), solid-liquid and quantum unbinding as well as superfluidity can be expected to exhibit a similar behavior with the de Boer parameter as discussed here.[79,80]

ACKNOWLEDGMENTS

We are most grateful to Victoria Buch for providing us with a copy of her DPIMC program which made this study possible. We thank Dörte Blume, Jordi Boronat, and Jesús Navarro for several useful comments and Sascha Warnecke for his skillful assistance in evaluating and plotting the data.

APPENDIX: TABLES OF COMPARISONS OF ENERGIES, MOI, AND SUPERFLUID FRACTIONS FOR BOLTZMANN AND BOSE STATISTICS FOR N=13 AND 26 AND T=0.5 AND 1.5 K

See Tables IV–VII.

TABLE IV. Comparison of DPIMC and PIMC reduced energies per molecule in Kelvin calculated for Boltzmann and Bose statistics, respectively, for N=13 and T=0.5 K and different $\varepsilon/\varepsilon_0$ and de Boer parameters Λ^*.

ε (K)	$\varepsilon/\varepsilon_0$	Λ^*	Statistics	$-V^*(N)/N$	$KE^*(N)/N$	$-E^*(N)/N$	I_{cl} (amu Å^2) [a]	$(\langle A^2\rangle)^{1/2}$ (Å^2) [b]	SF[c]
⋯	⋯	0	Boltzmann	3.391	0.020	3.371	⋯	⋯	0
68.4	2.00	0.202	Boltzmann	1.912	0.829	1.083	⋯	⋯	0
68.4	2.00	0.202	Bose	1.756	0.786	0.971	115	36.17	0.90(0.30)
51.3	1.50	0.232	Boltzmann	1.675	0.830	0.839	⋯	⋯	0
51.3	1.50	0.232	Bose	1.657	0.830	0.827	123.2	38.12	0.99(0.10)
34.2	1.00	0.284	Boltzmann	1.256	0.748	0.508	⋯	⋯	0
34.2	1.00	0.284	Bose	1.194	0.686	0.508	163.5	45.33	1.03
25.65	0.75	0.328	Boltzmann	0.907	0.584	0.323	⋯	⋯	0
25.65	0.75	0.328	Bose	0.889	0.562	0.327	210.6	50.54	1.01
22.8	0.67	0.348	Boltzmann	0.791	0.533	0.257	⋯	⋯	0
22.8	0.67	0.348	Bose	0.779	0.514	0.264	220.5	52.68	1.05
17.1	0.50	0.402	Boltzmann	0.520	0.401	0.118	⋯	⋯	0
17.1	0.50	0.402	Bose	0.522	0.388	0.133	291.8	60.10	1.03

[a]I_{cl} is the classical moment of inertia defined in Eq. (7).
[b]This is the root mean square of the area defined in Eq. (6).
[c]SF is the superfluid fraction. Values greater than unity are due to numerical errors.

TABLE V. Comparison of DPIMC and PIMC reduced energies per molecule in Kelvin calculated for Boltzmann and Bose statistics, respectively, for N=13 and T=1.5 K and different $\varepsilon/\varepsilon_0$ and de Boer parameters Λ^*.

ε (K)	$\varepsilon/\varepsilon_0$	Λ^*	Statistics	$-V^*(N)/N$	$KE^*(N)/N$	$-E^*(N)/N$	I_{cl} (amu Å^2) [a]	$(\langle A^2\rangle)^{1/2}$ (Å^2) [b]	SF[c]
⋯	⋯	0	Boltzmann	3.352	0.059	3.293	⋯	⋯	0
68.4	2.00	0.202	Boltzmann	1.912	0.830	1.082	⋯	⋯	0
68.4	2.00	0.202	Bose	1.756	0.789	0.968	115	10.28	0.25(0.18)
51.3	1.50	0.232	Boltzmann	1.674	0.837	0.838	⋯	⋯	0
51.3	1.50	0.232	Bose	1.658	0.835	0.822	123.2	11.22	0.26(0.07)
34.2	1.00	0.284	Boltzmann	1.258	0.754	0.504	⋯	⋯	0
34.2	1.00	0.284	Bose	1.196	0.695	0.501	155.4	23.49	0.89(0.01)
25.65	0.75	0.328	Boltzmann	0.906	0.612	0.294	⋯	⋯	0
25.65	0.75	0.328	Bose	0.883	0.565	0.318	199	27.29	0.94
22.8	0.67	0.348	Boltzmann	0.773	0.556	0.217	⋯	⋯	0
22.8	0.67	0.348	Bose	0.764	0.516	0.248	231	130.35	1.15

[a]I_{cl} is the classical moment of inertia defined in Eq. (7).
[b]This is the root mean square of the area defined in Eq. (6).
[c]SF is the superfluid fraction. Values greater than unity are due to numerical errors.

TABLE VI. Comparison of DPIMC and PIMC reduced energies per molecule in Kelvin calculated for Boltzmann and Bose statistics, respectively, for N=26 and T=0.5 K and different $\varepsilon/\varepsilon_0$ and de Boer parameters Λ^*.

ε (K)	$\varepsilon/\varepsilon_0$	Λ^*	Statistics	$-V^*(N)/N$	$KE^*(N)/N$	$-E^*(N)/N$	I_{cl} (amu Å^2) [a]	$(\langle A^2\rangle)^{1/2}$ (Å^2) [b]	SF[c]
⋯	⋯	0	Boltzmann	3.352	0.059	3.293	⋯	⋯	0
68.4	2.00	0.202	Boltzmann	2.494	1.018	1.475	⋯	⋯	0
68.4	2.00	0.202	Bose	2.291	0.956	1.335	378.9	11.05	0.026(0.002)
51.3	1.50	0.232	Boltzmann	2.225	1.052	1.173	⋯	⋯	0
51.3	1.50	0.232	Bose	2.204	1.042	1.161	400	12.37	0.03(0.003)
34.2	1.00	0.284	Boltzmann	1.760	1.015	0.745	⋯	⋯	0
34.2	1.00	0.284	Bose	1.613	0.877	0.736	484.7	74.36	0.99(0.03)
25.65	0.75	0.328	Boltzmann	1.287	0.794	0.492	⋯	⋯	0
25.65	0.75	0.328	Bose	1.260	0.761	0.499	570	83.04	1
22.8	0.67	0.348	Boltzmann	1.141	0.738	0.404	⋯	⋯	0
22.8	0.67	0.348	Bose	0.996	0.708	0.412	614.6	87.41	1.03
17.1	0.50	0.402	Boltzmann	0.794	0.583	0.211	⋯	⋯	0
17.1	0.50	0.402	Bose	0.788	0.560	0.228	771	97.10	1.01

[a]I_{cl} is the classical moment of inertia defined in Eq. (7).
[b]This is the root mean square of the area defined in Eq. (6).
[c]SF is the superfluid fraction. Values greater than unity are due to numerical errors.

TABLE VII. Comparison of DPIMC and PIMC reduced energies per molecule in Kelvin calculated for Boltzmann and Bose statistics, respectively, for N=26 and T=1.5 K and different $\varepsilon/\varepsilon_0$ and de Boer parameters Λ^*.

ε (K)	$\varepsilon/\varepsilon_0$	Λ^*	Statistics	$-V^*(N)/N$	$KE^*(N)/N$	$-E^*(N)/N$	I_{cl} (amu Å^2) [a]	$(\langle A^2\rangle)^{1/2}$ (Å^2) [b]	SF[c]
⋯	⋯	0	Boltzmann	3.352	0.059	3.293	⋯	⋯	0
68.4	2.00	0.202	Boltzmann	2.494	1.018	1.476	⋯	⋯	0
68.4	2.00	0.202	Bose	2.290	0.957	1.333	379	9.41	0.058(0.016)
51.3	1.50	0.232	Boltzmann	2.226	1.052	1.174	⋯	⋯	0
51.3	1.50	0.232	Bose	2.205	1.045	1.160	400	6.12	0.023(0.001)
34.2	1.00	0.284	Boltzmann	1.759	1.015	0.744	⋯	⋯	0
34.2	1.00	0.284	Bose	1.600	0.927	0.731	474	34.09	0.60(0.07)
25.65	0.75	0.328	Boltzmann	1.297	0.832	0.465	⋯	⋯	0
25.65	0.75	0.328	Bose	1.257	0.765	0.492	568.2	46.32	0.94
22.8	0.67	0.348	Boltzmann	1.143	0.777	0.366	⋯	⋯	0
22.8	0.67	0.348	Bose	1.114	0.711	0.403	616.3	48.15	0.94

[a]I_{cl} is the classical moment of inertia defined in Eq. (7).
[b]This is the root mean square of the area defined in Eq. (6).
[c]SF is the superfluid fraction. Values greater than unity are due to numerical errors.

[1] P. Sindzingre, D. M. Ceperley, and M. L. Klein, Phys. Rev. Lett. **67**, 1871 (1991).
[2] D. Scharf, M. L. Klein, and G. J. Martyna, J. Chem. Phys. **97**, 3590 (1992).
[3] D. Scharf, G. J. Martyna, and M. L. Klein, Chem. Phys. Lett. **197**, 231 (1992).
[4] M. A. McMahon, R. N. Barnett, and K. B. Whaley, J. Chem. Phys. **99**, 8816 (1993).
[5] M. A. McMahon and K. B. Whaley, Chem. Phys. **182**, 119 (1994).
[6] F. Mezzacapo and M. Boninsegni, Phys. Rev. Lett. **97**, 045301 (2006).
[7] M. V. Rama Krishna and K. B. Whaley, Z. Phys D: At., Mol. Clusters **20**, 223 (1991).
[8] G. Tejeda, J. M. Fernández, S. Montero, D. Blume, and J. P. Toennies, Phys. Rev. Lett. **92**, 223401 (2004).
[9] S. Baroni and S. Moroni, ChemPhysChem **6**, 1884 (2005).
[10] R. Guardiola and J. Navarro, Phys. Rev. A **74**, 025201 (2006).
[11] E. Rabani and J. Jortner, J. Phys. Chem. B **110**, 18893 (2006).
[12] J. E. Cuervo and P.-N. Roy, J. Chem. Phys. **125**, 124314 (2006).
[13] J. Navarro and R. Guardiola, J. Low Temp. Phys. **148**, 857 (2007).
[14] F. Mezzacapo and M. Boninsegni, Phys. Rev. A **75**, 033201 (2007).
[15] J. I. Martínez, M. Isla, and J. A. Alonso, Eur. Phys. J. D **43**, 61 (2007).
[16] S. A. Khairallah, M. B. Sevryuk, D. M. Ceperley, and J. P. Toennies, Phys. Rev. Lett. **98**, 183401 (2007).
[17] R. Guardiola and J. Navarro, Cent. Eur. J. Phys. **6**, 33 (2008).
[18] J. E. Cuervo and P.-N. Roy, J. Chem. Phys. **128**, 224509 (2008).
[19] F. Mezzacapo and M. Boninsegni, Phys. Rev. Lett. **100**, 145301 (2008); J. Phys.: Condens. Matter **21**, 164205 (2009); J. Phys.: Conf. Ser. **150**, 032059 (2009).
[20] S. Warnecke, M. B. Sevryuk, D. M. Ceperley, J. P. Toennies, R. Guardiola, and J. Navarro, Eur. Phys. J. D **56**, 353 (2010).
[21] S. Grebenev, B. G. Sartakov, J. P. Toennies, and A. F. Vilesov, Europhys. Lett. **83**, 66008 (2008).
[22] S. Grebenev, B. G. Sartakov, J. P. Toennies, and A. F. Vilesov, Science **289**, 1532 (2000).
[23] Y. Kwon and K. B. Whaley, Phys. Rev. Lett. **89**, 273401 (2002).
[24] F. Paesani, R. E. Zillich, Y. Kwon, and K. B. Whaley, J. Chem. Phys. **122**, 181106 (2005).
[25] E. W. Becker, K. Bier, and W. Henkes, Z. Phys. **146**, 333 (1956); E. W. Becker, P. Lohse, and R. Klingelhöfer, Z. Naturforsch. A **17**, 432 (1962).
[26] S. Montero, J. H. Morilla, G. Tejeda, and J. M. Fernández, Eur. Phys. J. D **52**, 31 (2009).
[27] A. Kalinin, O. Kornilov, and J. P. Toennies (in preparation).
[28] E. L. Knuth, F. Schünemann, and J. P. Toennies, J. Chem. Phys. **102**, 6258 (1995).
[29] E. L. Knuth, S. Schaper, and J. P. Toennies, J. Chem. Phys. **120**, 235 (2004).
[30] K. von Haeften, T. Laarmann, H. Wabnitz, and T. Möller, J. Electron Spectrosc. Relat. Phenom. **106**, 199 (2000).
[31] K. Kuyanov-Prozument and A. F. Vilesov, Phys. Rev. Lett. **101**, 205301 (2008).
[32] R. E. Grisenti, R. A. Costa Fraga, N. Petridis, R. Dörner, and J. Deppe, Europhys. Lett. **73**, 540 (2006).
[33] J. de Boer, Physica (Amsterdam) **14**, 139 (1948).
[34] J. de Boer and B. S. Blaisse, Physica (Amsterdam) **14**, 149 (1948).
[35] I. F. Silvera and V. V. Goldman, J. Chem. Phys. **69**, 4209 (1978).
[36] U. Buck, F. Huisken, A. Kohlhase, D. Otten, and J. Schaefer, J. Chem. Phys. **78**, 4439 (1983).
[37] P. Diep and J. K. Johnson, J. Chem. Phys. **112**, 4465 (2000).
[38] R. J. Hinde, J. Chem. Phys. **128**, 154308 (2008).
[39] K. Patkowski, W. Cencek, P. Jankowski, K. Szalewicz, J. B. Mehl, G. Garberoglio, and A. H. Harvey, J. Chem. Phys. **129**, 094304 (2008).
[40] D. J. Wales, J. P. K. Doye, A. Dullweber, M. P. Hodges, F. Y. Naumkin, F. Calvo, J. Hernández-Rojas, and T. F. Middleton, The Cambridge Cluster Database, http://www-wales.ch.cam.ac.uk/CCD.html.
[41] F. Calvo, J. P. K. Doye, and D. J. Wales, J. Chem. Phys. **114**, 7312 (2001).
[42] C. Chakravarty, J. Chem. Phys. **103**, 10663 (1995).
[43] P. A. Frantsuzov, D. Meluzzi, and V. A. Mandelshtam, Phys. Rev. Lett. **96**, 113401 (2006).
[44] J. Deckman, P. A. Frantsuzov, and V. A. Mandelshtam, Phys. Rev. E **77**, 052102 (2008).
[45] J. Deckman and V. A. Mandelshtam, Phys. Rev. E **79**, 022101 (2009).
[46] J. Deckman and V. A. Mandelshtam, J. Phys. Chem. A **113**, 7394 (2009).
[47] G. J. Hanna and D. Blume, Phys. Rev. A **74**, 063604 (2006).
[48] M. Meierovich, A. Mushinski, and M. P. Nightingale, J. Chem. Phys. **105**, 6498 (1996).
[49] V. Buch, J. Chem. Phys. **100**, 7610 (1994).
[50] K. A. Gernoth, T. Lindenau, and M. L. Ristig, Phys. Rev. B **75**, 174204 (2007).
[51] D. M. Ceperley, Rev. Mod. Phys. **67**, 279 (1995).
[52] I. F. Silvera, Rev. Mod. Phys. **52**, 393 (1980).
[53] These values differ somewhat from those used in Refs. 46 and 41.
[54] W. C. Stwalley and L. H. Nosanow, Phys. Rev. Lett. **36**, 910 (1976).
[55] K. T. Tang and J. P. Toennies, J. Chem. Phys. **118**, 4976 (2003).
[56] R. Guardiola and J. Navarro, J. Chem. Phys. **128**, 144303 (2008).
[57] C. Chakravarty, Mol. Phys. **84**, 845 (1995).
[58] The classical Monte Carlo values at finite T could be calculated with the DPIMC program starting with the classical (T=0) values of Wales and coworkers (Ref. 40).
[59] M. D. Miller, L. H. Nosanow, and L. J. Parish, Phys. Rev. B **15**, 214 (1977).
[60] L. H. Nosanow, L. J. Parish, and F. J. Pinski, Phys. Rev. B **11**, 191 (1975).
[61] The quantity $\langle R_c^2\rangle^{1/2}/N$ is sometimes referred to as the radius of gyration.
[62] S. M. Apenko, Phys. Rev. B **60**, 3052 (1999).
[63] A comparison with the bulk liquid at 0.5 K is of course not possible since H_2 freezes below 13.8 K.
[64] The quantities $\langle r_p^2\rangle^{1/2}$ and $\langle R_c^2\rangle^{1/2}$ are defined in the following way: $\langle r_p^2\rangle = (2/[N(N-1)])\Sigma_{i<j}(r_i-r_j)^2$ and $\langle R_c^2\rangle = (1/N)\Sigma_i(r_i-R)^2$, where $R = (1/N)\Sigma_i r_i$. Next it is noted that the sums in the two expressions are related, $2\Sigma_{i<j}(r_i-r_j)^2 = \Sigma_{i,j}(r_i-r_j)^2 = \Sigma_{i,j}([r_i-R]-[r_j-R])^2 = 2N\Sigma_i(r_i-R)^2$. Thus $\langle r_p^2\rangle^{1/2} = \sqrt{2N/(N-1)}\langle R_c^2\rangle^{1/2}$. The ratio $\langle r_p^2\rangle^{1/2}/\langle R_c^2\rangle^{1/2}$ is 1.47 for N=13, 1.44 for N=26 and approaches $\sqrt{2}$ with increasing N.
[65] C. Cazorla and J. Boronat, J. Phys.: Condens. Matter **20**, 015223 (2008).
[66] G. Pettersen and E. Østgaard, J. Low Temp. Phys. **70**, 279 (1988).
[67] C. Cazorla and J. Boronat, Phys. Rev. B **77**, 024310 (2008).
[68] L. A. Schwalbe, R. K. Crawford, H. H. Chen, and R. A. Aziz, J. Chem. Phys. **66**, 4493 (1977).
[69] In the early calculations of de Boer and Zucker [I. J. Zucker, Proc. Phys. Soc. **77**, 889 (1961)] values of ε current at the time were used with bulk total energies similar to the ones in Refs. 66–68. In the classical limit $\Lambda^*=0$ they obtained $E^*(N)/N=8.610$ instead of about 7.0 shown in Fig. 10. Thus it would seem that the earlier value is incorrect. However, in a recent PIMC calculation of solid H_2 by Chakravarty [C. Chakravarty, J. Chem. Phys. **116**, 8938 (2002)] in which Λ^* was varied by increasing m a limiting value of about 8.6 is obtained if her data at 18 and 4.2 K are extrapolated to 0 K. We have no explanation for the discrepancy to our value of 7.0.
[70] P. Slavíček, R. Kalus, P. Paška, I. Odvárková, P. Hobza, and A. Malijevský, J. Chem. Phys. **119**, 2102 (2003).
[71] A. Wüest and F. Merkt, J. Chem. Phys. **118**, 8807 (2003).
[72] K. T. Tang, J. P. Toennies, and C. L. Yiu, Phys. Rev. Lett. **74**, 1546 (1995).
[73] R. E. Grisenti, W. Schöllkopf, J. P. Toennies, G. C. Hegerfeldt, T. Köhler, and M. Stoll, Phys. Rev. Lett. **85**, 2284 (2000).
[74] J. Boronat, A. Fabrocini, and A. Polls, Phys. Rev. B **39**, 2700 (1989).
[75] M. L. Klein and J. A. Venables, *Rare Gas Solids* (Academic, London, 1976), Vol. 1, pp. 30, 333, and 464; *Rare Gas Solids* (Academic, London, 1977), Vol. 2, pp. 754, 762, and 763.
[76] V. G. Manzhelii and Y. A. Freiman, in *Physics of Cryocrystals*, edited by M. L. Klein and A. A. Maradudin (AIP, Woodbury, NY, 1997), p. 82.
[77] E. Tiesinga, B. J. Verhaar, and H. T. C. Stoof, Phys. Rev. A **47**, 4114 (1993).
[78] R. G. Palmer and P. W. Anderson, Phys. Rev. D **9**, 3281 (1974).
[79] D. M. Ceperley, G. V. Chester, and M. H. Kalos, Phys. Rev. D **13**, 3208 (1976).
[80] D. M. Ceperley, G. V. Chester, and M. H. Kalos, Phys. Rev. B **17**, 1070 (1978).